Effective small organic molecule as a defect passivator for highly efficient quasi-2D perovskite light emitting diodes

*Ying Li, Fuqiang Li, Zhongkai Yu, Vellaiappillai Tamilavan, Chang-Mok Oh, Woo Hyeon Jeong, Xinyu Shen, Seongbeom Lee, Xiangrui Du, Eunhye Yang, Yoomi Ahn, In-Wook Hwang, Bo Ram Lee, Sung Heum Park**

Ying Li, Fuqiang Li, Vellaiappillai Tamilavan, Seongbeom Lee, Xiangrui Du, Eunhye Yang, Yoomi Ahn, Sung Heum Park
Department of Physics, Pukyong National University, Busan, 48513, Republic of Korea

E-mail: spark@pknu.ac.kr

Ying Li, Fuqiang Li, Xiangrui Du, Eunhye Yang, Yoomi Ahn, Sung Heum Park
Institute of Energy Transport and Fusion Research, Pukyong National University, Busan, 48513, Republic of Korea

Zhongkai Yu, Woo Hyeon Jeong, Xinyu Shen, Bo Ram Lee
School of Advanced Materials Science and Engineering, Sungkyunkwan University (SKKU), Suwon, 16419, Republic of Korea

Chang-Mok Oh, In-Wook Hwang
Advanced Photonics Research Institute, Gwangju Institute of Science and Technology, Gwangju, 61005, Republic of Korea

Xinyu Shen
Clarendon Laboratory, Department of Physics, University of Oxford, Oxford OX1 3PU, U.K.

Keywords: defect passivation, quasi-2D, light-emitting diodes

Abstract

The use of a small organic molecular passivator has been proven to be a successful strategy for producing higher-performing quasi-2D perovskite light-emitting diodes (PeLEDs). The small organic molecule can passivate defects on the grain surround and surface of perovskite crystal structures, preventing nonradiative recombination and charge trapping. In this study, we report a new small organic additive called 2, 8-dibromodibenzofuran (diBDF) and

examines its effectiveness as a passivating agent in high-performance green quasi-2D PeLEDs. The oxygen atom in diBDF, acting as a Lewis base, forms coordination bonds with uncoordinated Pb^{2+}, so enhancing the performance of the device. In addition, the inclusion of diBDF in the quasi-2D perovskite results in a decrease in the abundance of low-n phases, hence facilitating efficient carrier mobility. Consequently, PeLED devices with high efficiency were successfully produced, exhibiting an external quantum efficiency of 19.9% at the emission wavelength of 517 nm and a peak current efficiency of 65.0 cd A^{-1}.

1. Introduction

Since their first fabrication in laboratories, perovskite light-emitting diodes (PeLEDs) have attracted enormous attention due to their excellent optoelectronic properties, such as high color purity, easily tunable composition, relatively low price, and so on, which give them the potential to be the next generation of display devices.[1-11] Although the highest records of external quantum efficiency (EQE) for PeLEDs are progressively converging towards the theoretical limit,[12-17] the functionality of these devices is still hindered by various issues, including intrinsic instability and low exciton binding energy typically observed in 3D perovskite materials.

Quasi-2D PeLEDs with quantum well structures facilitate overcoming the obstacles posed by their inherent instability and low exciton binding energy in 3D perovskites. [18-20] Due to the increased exciton binding energy, quasi-2D PeLEDs have superior efficiency and device stability when compared to 3D perovskite.[18, 21-23] The A sites of the perovskite crystal are partially occupied to form the quasi-2D structure by well-designed ammonium organic ligands, such as butylammonium (BA), 1-naphthylmethylammonium (NMA), and phenylethylammonium (PEA). These ligands coordinate with the "BX_6" octahedral structure, effectively controlling the vertical growth of the perovskite crystal and generating the formation of quantum well structures.[18-20] Among them, BA-based perovskite offers better processability than other aromatic ligands such as PEA^+.[24] The inclusion of BA^+ cation increases the device's reliability and repeatability. Furthermore, the addition of BABr has been observed to decrease the formation of the n = 1 phase,[25] which is advantageous for energy transfer in perovskite LED devices. Presently, various effective techniques have been employed in the development of highly efficient quasi-2D PeLEDs with full color coverage. These strategies encompass the control of crystal growth,[13, 26] modification of ligands,[24, 27-29] regulation of phases,[30, 31] optimization of transport layers,[26, 32-36] and additive engineering.[37-42] Among these, the introduction of a small organic molecular passivator has been demonstrated to be an effective method for achieving higher-performing devices. The small

organic molecule can effectively passivate defects on the grain boundary and surface of perovskite crystal structures, thereby inhibiting non-radiative recombination processes and charge trapping.

In this study, a novel small molecule organic additive, namely 2, 8-dibromodibenzofuran (diBDF), was introduced for direct incorporation into the perovskite precursor solution to passivate the defects formed in the grain boundaries and surface of perovskites active layer. The lone pair electrons on the oxygen atom of diBDF, acting as a Lewis base, can coordinate with the uncoordinated Pb^{2+}, thereby enhancing the performance of the devices. Furthermore, inserting the diBDF reduces the number of low-n phases in the quasi-2D perovskite, enabling efficient carrier transports. The quasi-2D PeLEDs produced by this strategy demonstrated peak current efficiencies of up to 65.0 cd A^{-1} and EQE of up to 19.9% at emission wavelengths of 517 nm.

2. Experimental section

2.1. Materials

A transparent conductive electrode composed of indium tin oxide (4.5 /sq ITO) was acquired from AMG. Poly(3, 4-ethylenedioxythiophene): poly-styrene sulfonate (PEDOT:PSS, Clevios Al 4083) was purchased from Heraeus Clevios, poly (9-vinlycarbazole) (PVK, Mw = 1, 100, 000 g mol^{-1}), 2, 8-dibromodibenzofuran (diBDF), lead bromide ($PbBr_2$, ≥98%), cesium bromide (CsBr, 99.999%), 18-Crown-6 ether (Crown, ≥99.0%), dimethyl sulfoxide (DMSO, 99.9%) and chlorobenzene (CB, 99.8%) were purchased from Sigma Aldrich. GreatCell Solar purchased *n*-Butylammonium bromide (BABr, 99.9%). Both 2, 2’, 2’’-(1, 3, 5-benzinetriyl) tris(1-phenyl-1-H-benzimidazole) (TPBi, 99.9%) and lithium fluoride (LiF, 99.9%) were purchased from OSM and iTASCO, respectively. All chemicals were utilized without any additional purification.

2.2. Preparation of Perovskite Precursor and HTL Solutions

For the manufacture of the quasi-2D $BA_2Cs_{n-1}Pb_nBr_{3n+1}$ perovskite film, the following ingredients were used: 1 mL of DMSO, 23.1 mg of BABr, 23.1 mg of CsBr, 55.05 mg of $PbBr_2$, and 4.0 mg of crown with and without 3 mg of diBDF. Stirring was performed overnight at 60 °C. Before use, the completely reactive solution was filtered using a 0.20 μm hydrophilic filter. For the hole transport layer (HTL) solution, the 4 mg mL^{-1} of PVK were dissolved in chlorobenzene.

2.3 Devices fabrication

The ITO substrates underwent a cleaning process involving the use of detergent and deionized water, followed by sonication in acetone and ethanol for a duration of 15 minutes each. Following the drying process in an oven, the substrates underwent treatment using a UV-ozone plasma cleaner for a duration of 15 minutes in order to enhance their hydrophilic properties. The PEDOT:PSS solution was applied onto a cleaned ITO substrate using spin-coating technique at a speed of 4500 rpm for a duration of 40 seconds. Following the annealing process at a temperature of 140 °C for a duration of 10 minutes, the samples were subsequently moved into a glove box. Within this controlled environment, a solution of PVK was deposited onto the films of PEDOT:PSS using a spin-coating technique at a rotational speed of 4000 rpm for a duration of 40 seconds. The perovskite precursor solution was subsequently applied onto the PVK films using spin-coating technique. The spin-coating process involved two steps: first, the solution was spun at a speed of 500 rpm for a duration of 5 seconds, and then at a speed of 7000 rpm for 40 seconds. After the spin-coating, the samples were subjected to annealing at a temperature of 120 °C for a period of 5 minutes under a nitrogen glovebox. A sequential thermal evaporation approach was employed to deposit layers of TPBi (75 nm)), LiF (2 nm), and aluminum (Al) (100 nm) onto the perovskite film. This process was carried out within a thermal evaporation chamber under a pressure of approximately 1×10^{-6} Torr. Based on the surface area occupied by the aluminum electrode, the designated area of the unit device measures 0.135 cm^2.

2.4 Density Functional Theory calculation

The Castep program in Materials Studio is employed to perform DFT simulations. A kinetic energy cutoff of 570.0 eV is utilized. During the calculation process, the Perdew-Burke-Ernzerhof (PBE) exchange correlation functional is combined with the generalized gradient approximation (GGA). ABX_3 (100) is simulated using a (3 × 3) supercell with a vacuum size of 20 emm, where organic matter is adsorbed onto it. The self-consistent field convergence condition is set to 1×10^{-6}eV/Atom, and a Monkhorst-Pack K-point grid of 2 × 2 × 1 is selected.

2.4 Characterization

The atomic force morphology (AFM) measurement was conducted using a scanning probe microscope (Icon-PT-PLUS, RUKER). The measurement of scanning electronic microscopy (SEM) was conducted using a Field Emission Scanning Electron Microscope-Schottky type

(TESCAN/MIRA3 LMH) with a beam energy of 5 kV. The experimental procedure involved doing steady-state photoluminescence (PL) measurements utilizing a pulsed xenon light. The experimental procedure involved conducting time-resolved PL measurements using a helium-cadmium (He Cd) laser with a wavelength of 375 nm. The photoluminescence quantum yield (PLQY) was measured by an absolute photoluminescence quantum yield spectrometer (C11347) from HAMAMATSU. The *J-V-L* characteristics, EQE, and electroluminescence (EL) spectra were obtained by employing a Konica Minolta spectroradiometer (CS-2000) in conjunction with a Keithley 2400 source meter. The measurements of device properties were conducted in ambient air conditions while utilizing encapsulation. The UV-visible absorption spectra were obtained using a Varian Cary 5000 spectrophotometer. The X-ray photoelectron spectrometer from KRATOS Analytical Ltd. (AXIS SUPRA) with an Al Kα (1486.6 eV) X-ray source was utilized for XPS analysis. The infrared (IR) camera PI640 was used to detect the suface temprature distribution of LED devices.The X-ray diffraction (XRD) measurement was conducted using X-Ray Diffractometer(Rigaku/UltimaIV). The femtosecond transient absorption spectra and decay were measured using a home-made transient absorption spectrometer with a 1-kHz repetition rate femtosecond Ti:sapphire regenerative amplifier system (Hurricane, Spectra Physics), infrared optical parametric amplifier (OPA-800CF, Spectra Physics), and Ocean Insight spectrometers (oceanFX, QEPro, and NIRQUEST). More details on this system were previously reported.[43, 44]

3. Results and discussion

The fabrication process involved the construction of PeLED devices using the following layered structure: ITO/PEDOT:PSS/PVK/perovskite/TPBi/LiF/Al. The aforementioned structure is observable in the cross-sectional SEM as depicted in **Figure S1a**. The hole injection and transport layers, namely PEDOT:PSS and PVK, were sequentially applied onto the clear ITO substrate. Subsequently, the perovskite material was put onto the PVK layer, serving as the emitting layer. The perovskite layer consists of quasi-2D structures of $BA_2Cs_{n-1}Pb_nBr_{3n+1}$ film, both with and without the diBDF additive. In this context, the variable "n" denotes the number of "$PbBr_6$" layers present in the 2D perovskite. The perovskite layers underwent treatment using the encapsulation growth approach already devised in our earlier work.[45] Finally, the TPBi, LiF, and Al layer were formed by thermal evaporation onto the perovskite layer. In this process, TPBi served as the electron transport layer, LiF functioned as the injection layer for electrons, and Al was utilized as the cathode for the entire device.

Figure 1a illustrates the molecular structure of diBDF with emphasis on the furan ring unit. It is anticipated that the lone pair electrons on the oxygen within the furan ring will coordinate with the uncoordinated Pb^{2+} present on the grain boundaries within the perovskite crystal, as depicted in **Figure 1b**. As a result, the formation of perovskite thin films with reduced defect density is expected.

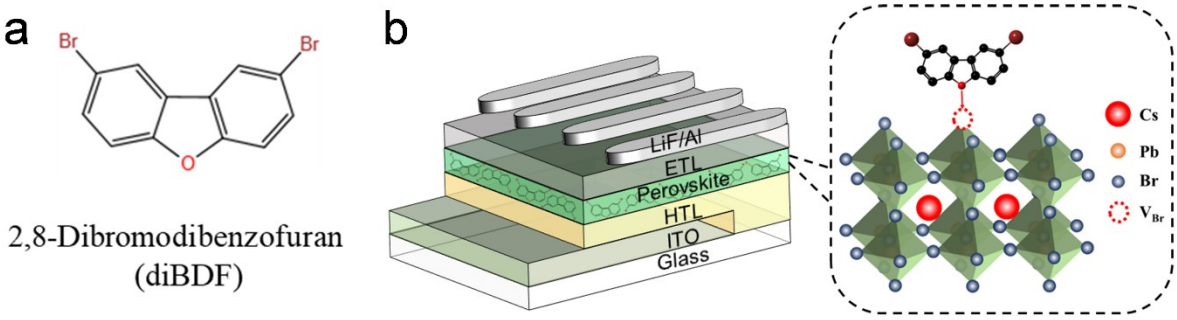

Figure 1. (a) Molecular structure of diBDF. (b) Schematic diagram for the mechanism of diBDF passivation.

Figure 2a displays the simulated electrostatic potential (ESP) surfaces of diBDF, exhibiting the 3D view of the charge distribution. The oxygen atom on the furan ring and the bromine atoms attached to the aromatic ring exhibit significant negative electron-withdrawing effects, resulting in higher Lewis basicity and increased potential as a passivator. In order to conduct a more comprehensive analysis of the interaction between the additional agent and perovskite, Fourier transform infrared spectroscopy (FTIR) was employed to assess the properties of perovskite thin films in the presence and absence of diBDF. As depicted in **Figure 2b**, the two prominent peaks associated with the C-O-C stretching vibration, positioned at 1210 cm^{-1} and 1075 cm^{-1}, have both undergone a shift. This shift can be interpreted as compelling evidence supporting the coordination of diBDF with uncoordinated Pb^{2+}, as well as the effective mitigation of defects within the perovskite crystal structure.[38, 40] In contrast, the peak associated with C-Br stretching did not exhibit any shift (see **Figure S2**), indicating that the interaction between the perovskite crystal and the diBDF compound was primarily mediated by the “O” atom on the furan ring rather than the “Br” atom.

In order to evaluate the impact of diBDF cooperation, X-ray photoelectron spectroscopy (XPS) was utilized to quantitatively measure alterations in electron cloud density. **Figure 2c** depicts the XPS result for the Pb element in both untreated and diBDF-treated perovskite thin films. The core levels Pb^{2+} spectrum in both $4f_{7/2}$ and $4f_{5/2}$ orbitals exhibit a clear shift to lower binding energy. Furthermore, the $3d_{3/2}$ and $3d_{5/2}$ orbitals of Br^- also shifted to lower binding energy (**Figure S3**), indicating that the introduction of diBDF can donate its lone electron

pairs to coordinate with the uncoordinated Pb^{2+} and influence the chemical environment of the ions in perovskite. This finding agrees with the FTIR measurements. Density functional theory (DFT) calculations are also undertaken to determine the mechanism of passivation of diBDF with $CsPbBr_3$ perovskite crystal as shown in **Figure 2d**. The (100) slab of the cubic $CsPbBr_3$ terminated by Cs and Br atoms with a Br vacancy on the surface was selected as the crystal model. Due to the scarcity of the Br atom, the subsurface Pb atom becomes unsaturated, resulting in a non-radiative combination. According to the DFT simulation, the diBDF can be adsorbed and coordinated with the uncoordinated Pb by electron donation. The adsorption energy was calculated from the formula: $E(ads) = E_{(diBDF+pero)} - E_{(pero)} - E_{(diBDF)}$, where $E_{(diBDF+pero)}$ is the total energy of the diBDF molecules adsorbed on the (100) plane of the perovskite crystal. $E_{(pero)}$ is the (100) plane energy of perovskite, and $E_{(diBDF)}$ is the diBDF molecule energy (the values of $E_{(diBDF+pero)}$, $E_{(pero)}$, and $E_{(diBDF)}$ are listed in **Table S1**). As a result, the adsorption energy of diBDF on $CsPbBr_3$ was found to be as high as 0.95 eV. This shows that diBDF has a strong ability to bind to the perovskite through an electron donation-acceptance interaction[46]

The evaluation of film morphologies of perovskite thin films, which were coated over a PVK layer, was conducted using atomic force microscopy (AFM). As shown in **Figures 2e** and **f**, the root mean roughness (RMS) of thin films containing diBDF is approximately 4.08 nm, indicating a significant improvement in films without diBDF (which are approximately 5.81 nm). The results obtained from the top-view SEM analysis as depicted in **Figure S1b** and **S1c**, along with the AFM findings, indicate that the incorporation of diBDF leads to the formation of thin films with enhanced uniformity and comprehensive coverage. These characteristics are advantageous for the performance of the devices and have the potential to reduce the leakage current in PeLEDs.[47, 48] Besides, the bright spots on the AFM images are speculated to be the $PbBr_2$ crystal,[49] and the decreased quantities of them could indicate the decrease of the uncoordinated Pb^{2+} ions defects.

The crystal structure of the perovskite thin films with and without diBDF were then detected through X-ray diffraction (XRD) to investigate the influence of diBDF on the perovskite crystallization. As the XRD patterns shown in **Figure S4**, after treated with the diBDF, the diffraction peak positions of the perovskite film remained unchanged. This phenomenon indicates that diBDF only acts as the ligand to coordinate with Pb^{2+} and does not enter the crystal lattice[49].

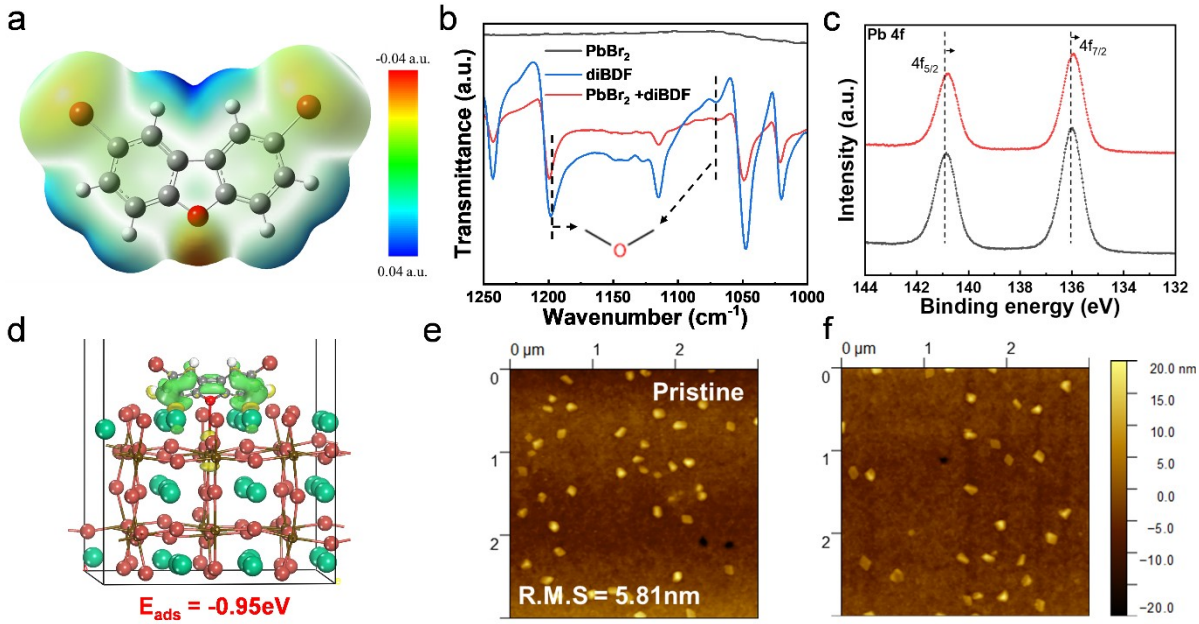

Figure 2. (a) Visualization of the ESP result of diBDF molecule. (b) FTIR spectra of powdered $PbBr_2$, diBDF and diBDF with $PbBr_2$. (c) XPS spectra for Pb $4f_{7/2}$ and Pb $4f_{5/2}$ of pristine and diBDF-treated perovskite films. (d) Adsorption configuration of diBDF on the Br-vacant- $CsPbBr_3$ surface. AFM morphology of (e) pristine and (f) diBDF treated perovskite films on PVK films.

The steady-state PL results for the perovskite film, both with and without diBDF, are depicted in **Figure 3a**. The perovskite film containing the diBDF compound demonstrates a notable increase in PL intensity. The increase in brightness can be readily seen with the naked eye when ultraviolet light with a wavelength of 365 nm excites the films (see the insets). Furthermore, the diBDF-treated perovskite material has a much higher PL quantum yield (PLQY) of roughly 78.1% in contrast to the pure perovskite thin films, which display a PLQY of about 49.6% (refer to **Figure S5**).

In the meantime, time-correlated single photon counting (TCSPC) measurements were performed on perovskite thin films with and without diBDF to determine the PL decay time change. The decay parameters were extracted by fitting the TCSPC curves (shown in **Figure 3b**) with the triexponential function: $I(\tau) = A_1 \exp(-t/\tau_1) + A_2 \exp(-t/\tau_2) + A_3 \exp(-t/\tau_2)$ for the pristine and diBDF-incorporated perovskite films. As a result, the average PL lifetime (τ_{avg}) of diBDF-treated perovskite was increased to τ_{avg} = 60.6 ns compared to τ_{avg} = 52.8 ns of the pristine films (detailed information is summarized in **Table S2**). The extended lifetime implies a reduction in defect density and the enhancement of radiative recombination in the diBDF-treated quasi-2D perovskite film, aligning with the observed increase in photoluminescence intensity.[42, 50] These results illustrate the compensation of Br^- vacancies

in the "$PbBr_6$" octahedral, which act as defect centers, by the lone pair electrons on diBDF. This compensation leads to a decrease in defect density and suppression of non-radiative recombination caused by the defects. **Figure 3c** depicts the UV-visible absorption spectra of the perovskite films prior to and subsequent to the application of diBDF treatment. The effective suppression of the n = 1 phase in the perovskite thin film is attributed to the design of the perovskite structure and the utilization of BA ligand.[25] However, the phases with n = 2 and n = 3 are still present. The introduction of diBDF into perovskite resulted in a decrease in the intensity of all peaks associated with low-dimensional domains (n = 1, 2, and 3). Notably, the ratio of the n=1 phase also decreased. Those suppressions agree with the low-n region observed in the PL spectra (**Figure S6**). Decrease in low dimensional domains is advantageous for energy transfer in quasi-2D perovskite and is ascribed as one of the reasons why our additive improves device efficiency.[51] The energy transfer process in the perovskite thin films with and without diBDF were further investigated with transient absorption spectra (TAS). As shown in **Figure S7**, the n = 3 domain showed very short-lived photobleach (PB) band of less than 1 ps, and n ≥ 4 domains appeared ~ 1 ps TA signal rise-time and long-lived PB band signal of over 100 ps. In the visualized TA kinetics traces (**Figure S7c**), the formation (rise) time constant (τ_{rise}) for PB n ≥ 4 in pristine film is 930 fs while the decay kinetics for PB n ≥ 4 peak of diBDF-treated perovskite film shows a shorter formation time of 740 fs, demonstrating the acceleration of energy transfer in quasi-two-dimensional perovskite films with optimized phase distribution.[40]

In order to conduct a more precise comparison of defect density between the pristine and treated devices, we utilized the space charge limited current (SCLC) measurement technique to determine the defect state density (N_t) for the hole-only devices with the structure of ITO/PEDOT:PSS/PVK/perovskite/MoO_3/Ag. The following formula was used to calculate the defect density: $N_t = \frac{2\varepsilon_0 \varepsilon V_{TFL}}{e L^2}$. Among them, ε denotes the relative dielectric constant of perovskite, ε_0 represents the vacuum permittivity, e signifies the elementary charge, L corresponds to the thickness of the perovskite film, and V_{TFL} denotes the trap-filled limit voltage. As demonstrated in **Figures 4a** and **b**, the V_{TFL} of the perovskite film treated with diBDF is measured to be 1.30 V, which represents a notable decrease compared to the voltage of 0.90 V observed in the original, untreated perovskite film. The lower V_{TFL} value represents fewer defects in the perovskite crystal,[34] which quantifies the passivation effect of the diBDF agent.

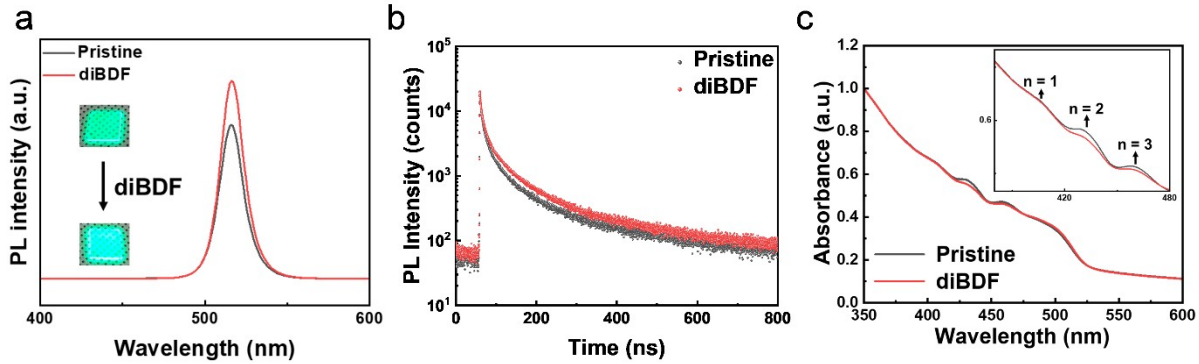

Figure 3. (a) Steady-state PL spectra (insert: the photographs of perovskite thin films under excitation of 365 nm ultraviolet light before and after introducing diBDF). (b) Time-resolved PL decay spectra of the perovskite thin films with and without diBDF, and (c) UV-Visible absorption spectra of pristine and diBDF-treated perovskite thin films.

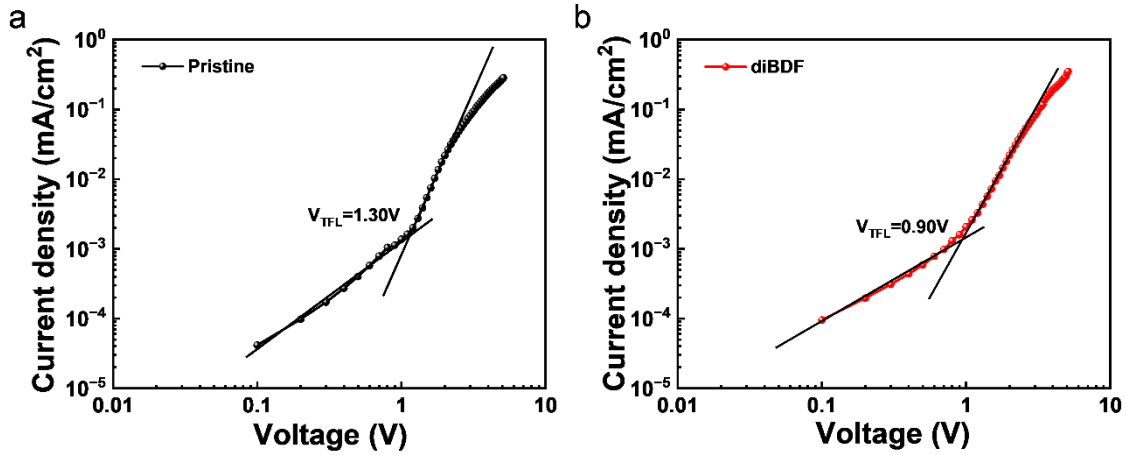

Figure 4. Current density-voltage characteristics of hole-only devices utilized for estimating the defect density in (a) pristine and (b) diBDF-treated perovskite films.

Figure 5a displays the current density-voltage-luminance (*J-V-L*) curves of the quasi-2D PeLEDs with and without diBDF treatment. Both pristine and treated devices demonstrate a significantly low level of leakage current, indicating the exceptional quality of our device. Furthermore, the luminance of the diBDF-treated devices increased in comparison to the pristine devices; the maximum luminance of the diBDF-treated device is 4650 cd m^{-2}, whereas the pristine device has a value of 4012 cd m^{-2}. In the identical experimental conditions, the EQE of our champion device incorporating diBDF has exhibited a notable enhancement, rising from 14% to 19.9% as illustrated in **Figure 5b**. Additionally, the current efficiency has experienced a substantial rise, progressing from 45.2 cd A^{-1} to 65.0 cd A^{-1} (**Figure S8**).

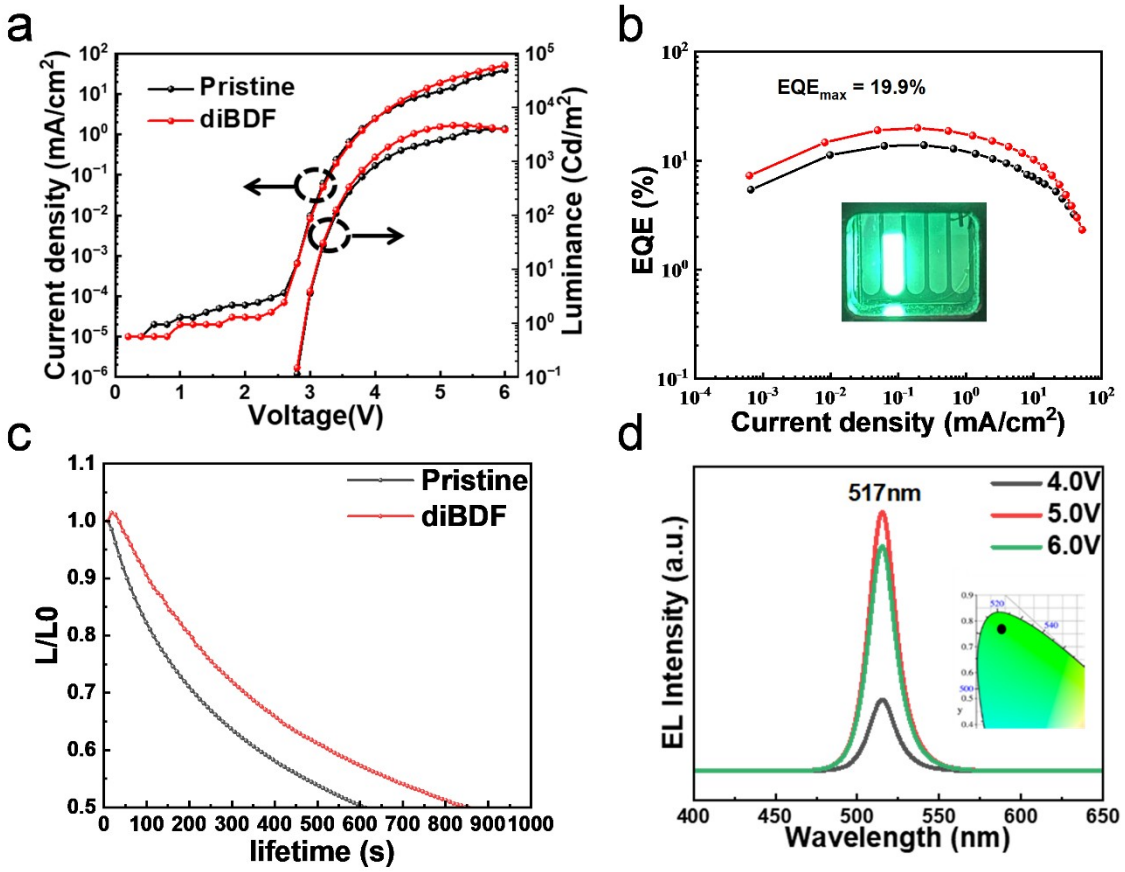

Figure 5. (a) *J*-*V* and luminance-voltage curves, (b) *J*-EQE curve (insert: the photograph of a sample of a device under the operational voltage), (c) Operating lifetimes at constant current density with an initial luminance of 100 cd m^{-2}, (d) EL spectra of a PeLED under various applied vias (insert: CIE coordinates).

In order to evaluate the operational stability, the lifetimes of the devices with and without the presence of diBDF were analyzed. **Figure 5c** demonstrates that the device incorporating the diBDF additive exhibited superior operational stability compared to the pristine devices. Specifically, the half-lifetime of the perovskite device treated with diBDF reached 855 s, with an initial luminance of approximately 100 cd m^{-2}. This represents an improvement of nearly 40% compared to the pristine device, which had a half-lifetime of approximately 612 s. The enhanced operational stability can be attributed to the passivation of defects present on the grain boundaries of the perovskite crystalline structure. This passivation process effectively suppresses ion migration and retards the degradation of device performance.[38, 39] Meanwhile, we used an IR camera to track and compare the surface temperatures of LED devices treated with and without diBDF (**Figure S9**). The surface temperature of the diBDF-treated device ultimately reached 22.78 °C after being powered at a constant voltage of 5.4 V, which is noticeably lower than the pristine devices' (25.14 °C) temperature. The reduction of the

temperature resulted from the decreased Joule heating produced by non-radiative recombination.[37, 52, 53] These findings could be interpreted as additional intuitive proof of diBDF's passivation impact, as well as a cause for diBDF to extend the lifetime of perovskite LEDs. In addition, the treated devices have a significant degree of stability at a specific wavelength of 517 nm, even under conditions of elevated operating voltage as illustrated in **Figure 5d**. The inset photo provides a visual representation of the device's position within the Commission Internationale de l'Eclariage (CIE) 1931 gamut coordinates. The comprehensive performance analysis is described in **Table 1** and **Figure S8.** The histogram analysis comparing the PeLEDs with and without diBDF clearly exhibits a notable improvement observed in the treated devices. This discovery highlights the robust reproducibility of the technique proposed in this study.

Table 1. Performance characteristics of the pristine and champion treated devices.

Sample configuration	Lmax [cd m^{-2}] @ bias	CEmax [cd A^{-1}] @ bias	EQEmax [%] @ bias	Wavelength [nm]
Pristine	4012.5 @ 6.0	45.2 @ 3.4	13.87 @ 3.4	517
diBDF	4650.5 @ 5.4	65.0 @ 3.4	19.90 @ 3.4	517

Furthermore, we investigated alternative passivation agents that possess a similar structure to diBDF. These agents include 2, 8-dibromodibenzothiophene (DBDBT), which contains a thiophene ring, and 3, 6-dibromocarbazole (DBCB), which features a carbazole ring. The structures of DBDBT and DBCB can be found in **Figure S10.** We conducted this comparison to assess the effectiveness of these agents as passivators. Based on the 3D views of the charge distribution of the molecules as depicted in **Figure S11**, the diBDF exhibits the highest electrostatic potential density on its heterocyclic ring when compared to DBDBT and DBCB. Consequently, diBDF may be regarded as possessing the most pronounced Lewis basicity among the three additives. **Figure S12** displays the SEM and AFM images of pristine and perovskite thin films treated with the agents and coated on a PVK layer. Among those images, it is obvious that the perovskite thin film treated with diBDF exhibits the highest level of uniformity and smoothness. Then, we fabricated LED devices containing these three additives in order to evaluate their electric properties. As the results, diBDF-treated LED device shows the highest EQE and the best operational stability among its analogues (**Figure S13** and **Table S3**). These results can be attributed to the fact that diBDF is more likely to donate its

lone pair electrons to the defect-abundant perovskite than other analogues and can therefore passivate the defects and enhance the performance of the PeLEDs more effectively. In addition, the V_{TFL} values of SCLC characterization for devices treated by different additives shows the same trend as we speculated (**Figure S14**), and the most reduced V_{TFL} value demonstrate the diBDF- treated device has the lowest defect density, which is consistent with the device performance.

4. Conclusion

In summary, we have effectively employed a small molecular organic additive known as diBDF, which possesses an abundance of lone electron pairs to improve the performance of PeLEDs. The lone pair electrons on the diBDF have the ability to establish coordination bonds with uncoordinated Pb^{2+}. This interaction between diBDF and Pb^{2+} has the potential to improve the overall performance of the devices. In addition, the incorporation of diBDF into the quasi-2D perovskite structure results in a decrease in the abundance of low-n phases, hence facilitating effective carrier transport. The PeLEDs fabricated using this approach exhibited a significant enhancement in device performance, with a brightness of 4650 cd m^{-2} at 517 nm and an EQE of 19.9%, compared to 4012 cd m^{-2} and 13.8% for the untreated device. Our findings suggest that an efficient small molecule additive can be used to fabricate high-performance quasi-2D perovskite emission devices.

Supporting Information

Supporting Information is available from the Wiley Online Library or from the author.

Acknowledgements

Y. Li and F. Q. Li contributed equally to this work. This research was supported by the BrainLink program (2022H1D3A3A01077343) and the Nano Material Technology Development Program (2021M3H4A1A02057007) funded by the Ministry of Science and ICT through the National Research Foundation of Korea. This research was supported by the Basic Science Research Program through the NRF funded by the Ministry of Education (2022R1A6A1A03051158).

Received: ((will be filled in by the editorial staff))
Revised: ((will be filled in by the editorial staff))
Published online: ((will be filled in by the editorial staff))

References

[1] Tan, Z.-K.; Moghaddam, R. S.; Lai, M. L.; Docampo, P.; Higler, R.; Deschler, F.; Price, M.; Sadhanala, A.; Pazos, L. M.; Credgington, D.; Hanusch, F.; Bein, T.; Snaith, H. J.; Friend, R. H., *Nat. Nanotechnol.* **2014,** *9,* 687.

[2] Zhang, L.; Sun, C.; He, T.; Jiang, Y.; Wei, J.; Huang, Y.; Yuan, M., *Light Sci. Appl.* **2021,** *10,* 61.

[3] Ji, K.; Anaya, M.; Abfalterer, A.; Stranks, S. D., *Adv. Opt. Mater.* **2021,** *9,* 2002128.

[4] Wu, X.; Trinh, M. T.; Niesner, D.; Zhu, H.; Norman, Z.; Owen, J. S.; Yaffe, O.; Kudisch, B. J.; Zhu, X. Y., *J. Am. Chem. Soc.* **2015,** *137,* 2089.

[5] Lai, H.; Kan, B.; Liu, T.; Zheng, N.; Xie, Z.; Zhou, T.; Wan, X.; Zhang, X.; Liu, Y.; Chen, Y., *J. Am. Chem. Soc.* **2018,** *140,* 11639.

[6] Yukta; Satapathi, S., *ACS Appl. Electron. Mater*. **2022,** *4,* 1469.

[7] Liang, C.; Gu, H.; Xia, J.; Mei, S.; Pang, P.; Zhang, N.; Guo, J.; Guo, R.; Shen, Y.; Yang, S.; Wei, Z.; Shao, G.; Xing, G., *Adv. Funct. Mater.* **2022,** *32,* 2108926.

[8] Jeong, J.-E.; Park, J. H.; Jang, C. H.; Song, M. H.; Woo, H. Y., *Adv. Mater.* **2020,** *32,* 2002176.

[9] Li, N.; Jia, Y.; Guo, Y.; Zhao, N., *Adv. Mater.* **2022,** *34,* 2108102.

[10] Ren, A.; Wang, H.; Zhang, W.; Wu, J.; Wang, Z.; Penty, R. V.; White, I. H., *Nat. Electron.* **2021,** *4,* 559.

[11] Fu, L.; Li, H.; Wang, L.; Yin, R.; Li, B.; Yin, L., *Energy Environ. Sci.* **2020,** *13,* 4017.

[12] Bai, W.; Xuan, T.; Zhao, H.; Dong, H.; Cheng, X.; Wang, L.; Xie, R.-J., *Adv. Mater.* **2023,** *35,* 2302283.

[13] Kim, J. S.; Heo, J.-M.; Park, G.-S.; Woo, S.-J.; Cho, C.; Yun, H. J.; Kim, D.-H.; Park, J.; Lee, S.-C.; Park, S.-H.; Yoon, E.; Greenham, N. C.; Lee, T.-W., *Nature* **2022,** *611,* 688.

[14] Zhou, W.; Shen, Y.; Cao, L.-X.; Lu, Y.; Tang, Y.-Y.; Zhang, K.; Ren, H.; Xie, F.-M.; Li, Y.-Q.; Tang, J.-X., *Adv. Funct. Mater.* **2023,** *33,* 2301425.

[15] Jiang, Y.; Sun, C.; Xu, J.; Li, S.; Cui, M.; Fu, X.; Liu, Y.; Liu, Y.; Wan, H.; Wei, K.; Zhou, T.; Zhang, W.; Yang, Y.; Yang, J.; Qin, C.; Gao, S.; Pan, J.; Liu, Y.; Hoogland, S.; Sargent, E. H.; Chen, J.; Yuan, M., *Nature* **2022,** *612,* 679.

[16] Jiang, J.; Chu, Z.; Yin, Z.; Li, J.; Yang, Y.; Chen, J.; Wu, J.; You, J.; Zhang, X., *Adv. Mater.* **2022,** *34,* 2204460.

[17] Shen, X.; Kang, K.; Yu, Z.; Jeong, W. H.; Choi, H.; Park, S. H.; Stranks, S. D.; Snaith, H. J.; Friend, R. H.; Lee, B. R., *Joule* **2023,** *7,* 272.

[18] Zhu, L.; Liu, D.; Wang, J.; Wang, N., *J. Phys. Chem. Lett.* **2020,** *11,* 8502.

[19] Zhu, Z.; Zhu, C.; Yang, L.; Chen, Q.; Zhang, L.; Dai, J.; Cao, J.; Zeng, S.; Wang, Z.; Wang, Z.; Zhang, W.; Bao, J.; Yang, L.; Yang, Y.; Chen, B.; Yin, C.; Chen, H.; Cao, Y.; Gu, H.; Yan, J.; Wang, N.; Xing, G.; Li, H.; Wang, X.; Li, S.; Liu, Z.; Zhang, H.; Wang, L.; Huang, X.; Huang, W., *Nat. Mater.* **2022,** *21,* 1042.

[20] Yang, S.; Dai, J.; Yu, Z.; Shao, Y.; Zhou, Y.; Xiao, X.; Zeng, X. C.; Huang, J., *J. Am. Chem. Soc.* **2019,** *141,* 5781.

[21] Guo, K.; Li, W.; He, Y.; Feng, X.; Song, J.; Pan, W.; Qu, W.; Yang, B.; Wei, H., *Angew. Chem. Int. Ed.* **2023,** *62,* e202303445.

[22] Yang, X.; Zhang, X.; Deng, J.; Chu, Z.; Jiang, Q.; Meng, J.; Wang, P.; Zhang, L.; Yin, Z.; You, J., *Nat. Commun.* **2018,** *9,* 570.

[23] Leung, T. L.; Ahmad, I.; Syed, A. A.; Ng, A. M. C.; Popović, J.; Djurišić, A. B., *Commun. Mater.* **2022,** *3,* 63.

[24] Leung, T. L.; Tam, H. W.; Liu, F.; Lin, J.; Ng, A. M. C.; Chan, W. K.; Chen, W.; He, Z.; Lončarić, I.; Grisanti, L.; Ma, C.; Wong, K. S.; Lau, Y. S.; Zhu, F.; Skoko, Ž.; Popović, J.; Djurišić, A. B., *Adv. Opt. Mater.* **2020,** *8,* 1901679.

[25] Jin, G.; Liu, T.; Li, Y.; Zhou, J.; Zhang, D.; Pang, P.; Ye, Z.; Xing, Z.; Xing, G.; Chen, J.; Ma, D., *Nanoscale* **2022,** *14,* 919.

[26] Shen, Y.; Wu, H.-Y.; Li, Y.-Q.; Shen, K.-C.; Gao, X.; Song, F.; Tang, J.-X., *Adv. Funct. Mater.* **2021,** *31,* 2103870.

[27] Jae Do, J.; Chung, Y.; Kim, K. S.; Kim, D. H.; Jung, J. W., *J. Alloys Compd.* **2023,** *940,* 168913.

[28] Liu, Y.; Cui, J.; Du, K.; Tian, H.; He, Z.; Zhou, Q.; Yang, Z.; Deng, Y.; Chen, D.; Zuo, X.; Ren, Y.; Wang, L.; Zhu, H.; Zhao, B.; Di, D.; Wang, J.; Friend, R. H.; Jin, Y., *Nat. Photonics* **2019,** *13,* 760.

[29] Ren, Z.; Li, L.; Yu, J.; Ma, R.; Xiao, X.; Chen, R.; Wang, K.; Sun, X. W.; Yin, W.-J.; Choy, W. C. H., *ACS Energy Lett.* **2020,** *5,* 2569.

[30] Hu, Y.; Spies, L. M.; Alonso-Álvarez, D.; Mocherla, P.; Jones, H.; Hanisch, J.; Bein, T.; Barnes, P. R. F.; Docampo, P., *J. Mater. Chem. A* **2018,** *6,* 22215.

[31] Li, H.; Hu, S.; Wang, H.; Zhang, X.; Tong, Y.; Qi, H.; Guo, P.; Zhao, G.; Gao, J.; Liu, P.; Zang, J.; Hao, H.; Liu, T.; Bian, H.; Zhang, Y.; Wei, Y.; Guo, Y.; Zhang, L.; Fang, Y.; Wang, H., *ACS Appl. Mater. Interfaces* **2023,** *15,* 9574.

[32] Chu, Z.; Zhang, W.; Jiang, J.; Qu, Z.; Ma, F.; Zhao, Y.; Chu, X.; Shen, Y.; Li, Y.; Yin, Z.; Zhang, X.; You, J., *Nature Electronics* **2023,** *6,* 360.

[33] Zhao, B.; Lian, Y.; Cui, L.; Divitini, G.; Kusch, G.; Ruggeri, E.; Auras, F.; Li, W.; Yang, D.; Zhu, B.; Oliver, R. A.; MacManus-Driscoll, J. L.; Stranks, S. D.; Di, D.; Friend, R. H., *Nat. Electron.* **2020,** *3*, 704.

[34] Gao, Y.; Liu, Y.; Zhang, F.; Bao, X.; Xu, Z.; Bai, X.; Lu, M.; Wu, Y.; Wu, Z.; Zhang, Y.; Wang, Q.; Gao, X.; Wang, Y.; Shi, Z.; Hu, J.; Yu, W. W.; Zhang, Y., *Adv. Mater.* **2022,** *34*, 2207445.

[35] Na Quan, L.; Ma, D.; Zhao, Y.; Voznyy, O.; Yuan, H.; Bladt, E.; Pan, J.; García de Arquer, F. P.; Sabatini, R.; Piontkowski, Z.; Emwas, A.-H.; Todorović, P.; Quintero-Bermudez, R.; Walters, G.; Fan, J. Z.; Liu, M.; Tan, H.; Saidaminov, M. I.; Gao, L.; Li, Y.; Anjum, D. H.; Wei, N.; Tang, J.; McCamant, D. W.; Roeffaers, M. B. J.; Bals, S.; Hofkens, J.; Bakr, O. M.; Lu, Z.-H.; Sargent, E. H., *Nat. Commun.* **2020,** *11*, 170.

[36] Yu, Z.; Jeong, W. H.; Kang, K.; Song, H.; Shen, X.; Ahn, H.; Lee, S. W.; Fan, X.; Jang, J. W.; Ha, S. R.; Min, J. W.; Park, J. H.; Han, J.; Jung, E. D.; Song, M. H.; Chang, D. W.; Im, W. B.; Park, S. H.; Choi, H.; Lee, B. R., *J. Mater. Chem. A* **2022,** *10*, 13928.

[37] Liu, Y.; Cai, L.; Xu, Y.; Li, J.; Qin, Y.; Song, T.; Wang, L.; Li, Y.; Ono, L. K.; Qi, Y.; Sun, B., *Nano Energy* **2020,** *78*, 105134.

[38] Zhang, D.; Fu, Y.; Zhan, H.; Zhao, C.; Gao, X.; Qin, C.; Wang, L., *Light Sci. Appl.* **2022,** *11*, 69.

[39] Zhao, C.; Wu, W.; Zhan, H.; Yuan, W.; Li, H.; Zhang, D.; Wang, D.; Cheng, Y.; Shao, S.; Qin, C.; Wang, L., *Angew. Chem. Int. Ed.* **2022,** *61*, e202117374.

[40] Kong, L.; Zhang, X.; Li, Y.; Wang, H.; Jiang, Y.; Wang, S.; You, M.; Zhang, C.; Zhang, T.; Kershaw, S. V.; Zheng, W.; Yang, Y.; Lin, Q.; Yuan, M.; Rogach, A. L.; Yang, X., *Nat. Commun.* **2021,** *12*, 1246.

[41] Ren, Z.; Sun, J.; Yu, J.; Xiao, X.; Wang, Z.; Zhang, R.; Wang, K.; Chen, R.; Chen, Y.; Choy, W. C. H., *Nanomicro Lett* . **2022,** *14*, 66.

[42] Ren, Z.; Yu, J.; Qin, Z.; Wang, J.; Sun, J.; Chan, C. C. S.; Ding, S.; Wang, K.; Chen, R.; Wong, K. S.; Lu, X.; Yin, W.-J.; Choy, W. C. H., *Adv. Mater.* **2021,** *33*, 2005570.

[43] Oh, C.-M.; Lee, J.; Park, S. H.; Hwang, I.-W., *Spectrochim. Acta A Mol. Biomol. Spectrosc.* **2021,** *250*, 119227.

[44] Oh, C.-M.; Lee, J.; Park, S. H.; Hwang, I.-W., *J. Phys. Chem. Lett.* **2021,** *12*, 6418-

[45] Liu, Y.; Yu, Z.; Chen, S.; Park, J. H.; Jung, E. D.; Lee, S.; Kang, K.; Ko, S.-J.; Lim, J.; Song, M. H.; Xu, B.; Snaith, H. J.; Park, S. H.; Lee, B. R., *Nano Energy* **2021,** *80*, 105511.

[46] Chen, H.; Liu, T.; Zhou, P.; Li, S.; Ren, J.; He, H.; Wang, J.; Wang, N.; Guo, S., *Adv. Mater.* **2020,** *32*, 1905661.

[47] Mishra, A.; Bose, R.; Zheng, Y.; Xu, W.; McMullen, R.; Mehta, A. B.; Kim, M. J.; Hsu, J. W. P.; Malko, A. V.; Slinker, J. D., *Adv. Mater.* **2022,** *34*, 2203226.

[48] Li, M.; Zhao, Y.; Qin, X.; Ma, Q.; Lu, J.; Lin, K.; Xu, P.; Li, Y.; Feng, W.; Zhang, W.-H.; Wei, Z., *Nano Lett.* **2022,** *22*, 2490.

[49] Qi, Z.; Yuan, L.; Ding, W.; Qin, Z.; Wang, S.; Liu, H.; Li, X., *Small n/a* (n/a), 2304821. DOI https://doi.org/10.1002/smll.202304821.

[50] Ma, J.; Yang, L.; Zhang, Y.; Kuang, Y.; Shao, M., *J. Phys. Chem. Lett.* **2022,** *13*, 4739

[51] Liu, Y.; Chen, F.; Jiang, Z.; Li, Y.; Zhou, X.; Wu, J.; Chen, S.; Zhang, L.; Li, Y.; Liu, C.; Bae, S.-H.; Lee, B. R.; Huang, B.; Wang, X.; Lee, Y. S.; Kim, J.; Park, S. H.; Yu, X.-F.; Xu, B., *Adv. Opt. Mater.* **2022,** *10*, 2200885.

[52] Shen, X.; Kwak, S. L.; Jeong, W. H.; Jang, J. W.; Yu, Z.; Ahn, H.; Park, H. J.; Choi, H.; Park, S. H.; Snaith, H. J.; Hwang, D.-H.; Lee, B. R., *Small* **2023,** *19*, 2303472.

[53] Liu, Y.; Ono, L. K.; Tong, G.; Zhang, H.; Qi, Y., *ACS Energy Lett.* **2021,** *6*, 908.

This work presents an organic small molecule additive as passivation material for PeLEDs, which reduces the defect density in the perovskite crystal hence improves the external quantum efficiency and stability of devices. This strategy effectively enhances the performance of PeLEDs.

Ying Li, Fuqiang Li, Zhongkai Yu, Vellaiappillai Tamilavan, Chang-Mok Oh, Woo Hyeon Jeong, Xinyu Shen, Seongbeom Lee, Xiangrui Du, Eunhye Yang, Yoomi Ahn, In-Wook Hwang, Bo Ram Lee, Sung Heum Park*

Effective small organic molecule as a defect passivator for highly efficient quasi-2D perovskite light emitting diodes